Mechanisms in Homogeneous Catalysis

A Spectroscopic Approach

Edited by
Brian Heaton

WILEY-VCH Verlag GmbH & Co. KGaA

Mechanisms in Homogeneous Catalysis

Edited by
Brian Heaton

Further Titles of Interest

B. Cornils, W. A. Herrmann, R. Schlögl, C.-H. Wong (Eds.)

Catalysis from A to Z

A Concise Encyclopedia

2nd Edition
2003
ISBN 3-527-30373-1

I. Chorkendorff, J. W. Niemantsverdriet

Concepts of Modern Catalysis and Kinetics

2003
ISBN 3-527-30574-2

J. W. Niemantsverdriet

Spectroscopy in Catalysis

2nd Edition
2000
ISBN 3-527-30200-X

Mechanisms in Homogeneous Catalysis

A Spectroscopic Approach

Edited by
Brian Heaton

WILEY-VCH Verlag GmbH & Co. KGaA

Edited by

Prof. Dr. Brian Heaton
University of Liverpool
Department of Chemistry
Liverpool L69 7ZD
UK

Library of Congress Card No.: applied for

British Library Cataloguing-in-Publication Data:
A catalogue record for this book is available from the British Library.

Bibliographic information published by Die Deutsche Bibliothek
Die Deutsche Bibliothek lists this publication in the Deutsche Nationalbibliografie; detailed bibliographic data is available in the Internet at <http://dnb.ddb.de>.

Printed in the Federal Republic of Germany.
Printed on acid-free paper.

Typesetting hagedorn kommunikation, Viernheim
Printing betz-druck GmbH, Darmstadt
Bookbinding Litges & Dopf Buchbinderei GmbH, Heppenheim

ISBN-13: 978-3-527-31025-8
ISBN-10: 3-527-31025-8

Preface

This volume brings together leading international authors who have made important contributions to developing/applying NMR and IR spectroscopic methods to the study of a wide variety of industrial, homogeneous transition metal catalysed reactions used for the manufacture of high tonnage products (eg. aldehydes and alcohols) to lower volume, speciality chemicals. The spectroscopic identification of catalytic intermediates in the elucidation of the catalytic cycle, together with the rates and mechanisms of the individual steps, have long been of interest to both academic and industrial chemists. A better understanding of the catalytic cycle, using the two most widely applicable spectroscopic techniques-IR and NMR-in this area, has allowed improved overall rates of the catalytic reaction (sometimes it has been possible to even measure and improve the rates for individual steps in the catalytic cycle), selectivities and a reduction in by-product formation to be achieved through systematically varying ligand design, the metal, promoters and reaction conditions. In this way, many processes have been improved and new ones developed.

NMR is one of the most powerful methods for structural identification and for obtaining information about both the type and rate of inter- and intra-exchange processes; recent developments also allow information about diffusion and ion-pairing to be obtained. Detailed structural information in solution is possible from NMR measurements, since most of the elements in the Periodic Table can be used for NMR measurements. NMR no longer relies solely on variable temperature 1-D multinuclear measurements for the identification of catalytic species but a variety of 2-D NMR methods, using either 1-, 2- or 3-bond coupling constants, allow data to be obtained in a much more efficient manner. Thus, although rhodium complexes have long been known to be active catalysts, ^{103}Rh NMR data, hitherto, have been difficult to obtain because of the low sensitivity of ^{103}Rh; now, ^{103}Rh NMR data can be readily obtained, using 2-D HMQC methods, which rely upon ^{n}J(Rh-X) (X = ^{1}H, ^{13}C, ^{31}P, etc; n = 1, 2, 3). This, together with the vast armoury of NMR methods now applicable to the study of homogeneous catalysis, are dealt with in chapter 1 and, hopefully, this will allow the non-specialist NMR person to select and use the appropriate method to solve their particular problem.

One inherent problem with NMR is the relatively low sensitivity of the technique. Thus, for a reasonable S : N/collection time, it is necessary to use solutions of 10-100 mM, which is well above the concentrations (often <1 mM) used in catalytic experiments. As a result, species present in the catalytic solution can sometimes be different at the higher concentrations used for NMR measurements. However, for reactions involving H_2, the use of *p*-H_2 circumvents these problems and detection of species at very low concentrations is possible (chapters 1, 6 and 9).

IR spectroscopy is complementary to NMR and is especially useful for reactions involving M-CO's; it is suitable for the study of catalytic solutions, at the catalytic concentrations used, and has long been used to study catalytic reactions to identify species and obtain rates e. g. Forster's work at Monsanto in the 1970's when he successfully clarified the nature of the catalytic cycle for the rhodium-catalysed conversion of methanol to acetic acid. For M-CO's, it is much easier and quicker to obtain IR spectra containing υ(CO) bands than to obtain NMR spectra of even the most sensitive nucleus, ^{1}H, even at the highest magnetic fields now available. However, since the dispersion of υ(CO) bands is not very great, deconvolution of IR spectra and identification of species present in catalytic solutions has in the past been somewhat difficult. Garland has now introduced a powerful method (chapter 4) for the reconstruction of individual pure component IR spectra from complex component catalytic mixtures-the **B**and **T**arget **E**ntropy **M**inimisation (**BTEM**) protocol; this is an extremely powerful computational method, which presently allows recovery of pure component IR spectra of unknown species when present at very low concentrations. This method seems to be generally applicable and is being presently extended to include NMR, X-ray powder diffraction etc.

Many catalytic reactions require high pressures of reactant gases. Thus, an in-depth understanding of such catalytic systems requires ***truly in situ*** NMR and IR measurements and it has been necessary to develop appropriate High Pressure-spectroscopic cells; the development and use of HP-NMR and HP-IR cells are reviewed in chapters 2 and 3 respectively. The use of both of these complementary methods/HP-techniques is probably best illustrated in chapters 5 – carbonylation reactions, chapter 6 – hydroformylation and chapter 7 – alkene/CO copolymerisation, which deal with the recent advances in each of these important areas.

Over the last 20 years, there has been an enormous increase in the use of NMR spectroscopy in metallocene-based polymerisation catalysis and these studies have provided an unprecedented increase in our understanding; this has allowed the properties of homo- and co-polymers to be tailored and transition state energies to be lowered by 1-2 kcal mol^{-1}, which makes all the difference between a poor and a highly successful catalyst.

The increased knowledge about bonding, reactivity in organometallic chemistry has greatly contributed to our understanding of the possible mechanisms of catalysis and this, together with the advances/applications in NMR and IR techniques/cells described in this volume, has allowed catalytic mechanisms to be much better understood.

I hope this volume will transfer some important aspects of NMR and IR, including the use of HP-spectroscopic cells for measurements under actual reaction con-

ditions, to the homogeneous community. I would like to thank all the authors of the chapters for their valiant contributions in this area. However, despite much international effort, the complete spectroscopic identification of **all** the intermediates in any catalytic cycle has only so far been achieved for two reactions:- the hydrogenation described in chapter 8, which surprisingly involves an intermediate with an agostic-H, and the Pd-catalysed methoxycarbonylation of ethene, which we reported recently, described in chapter 1. So, there is still plenty of opportunity for identification of new mechanisms by people working in this area!

Liverpool, January 2004 Brian Heaton

Contents

List of Contributors

Claudio Bianchini
Institute of Chemistry of Organo-metallic Compounds, ICCCOM-CNR
Via J. Nardi 39
50132 Firenze
Italy

Manfred Bochmann
Wolfson Materials and Catalysis Centre
School of Chemical Sciences and Pharmacy
University of East Anglia
Norwich, NR4 7TJ
United Kingdom

Marc Garland
Department of Chemical and Biomolecular Engineering
4 Engineering Dr 4
National University of Singapore
Singapore 117576
Singapore

Ralf Giernoth
Institute of Organic Chemistry
University of Cologne
Greinstr. 4
50939 Köln
Germany

Anthony Haynes
Department of Chemistry
University of Sheffield
Dainton Building
Brook Hill
Sheffield, S3 7HF
United Kingdom

Lothar Helm
Institute of Chemical Sciences and Engineering, ISIC
Ecole polytechnique fédérale de Lausanne BCH
1015 Lausanne
Switzerland

Paul C. J. Kamer
van't Hoff Institute for Molecular Sciences
University of Amsterdam
Nieuwe Achtergracht 166
1018 WV Amsterdam
The Netherlands

Gábor Laurenczy
Institute of Chemical Sciences and Engineering, ISIC
Ecole polytechnique fédérale de Lausanne BCH
1015 Lausanne
Switzerland

Piet W. N.M. van Leeuwen
van t Hoff Institute for Molecular Sciences
University of Amsterdam
Nieuwe Achtergracht 166
1018 WV Amsterdam
The Netherlands

Andrea Meli
Institute of Chemistry of Organometallic Compounds, ICCCOM-CNR
Via J. Nardi 39
50132 Firenze
Italy

George Morris
BP-Amoco Chemicals
Saltend
Hull HU12 8DS
United Kingdom

Paul S. Pregosin
Laboratory of Inorganic Chemistry
ETHZ HCI Hönggerberg
8093 Zurich
Switzerland

Paul C. J. Reek
van t Hoff Institute for Molecular Sciences
University of Amsterdam
Nieuwe Achtergracht 166
1018 WV Amsterdam
The Netherlands

Daniele Schott
Laboratory of Inorganic Chemistry
ETHZ HCI Hönggerberg
8093 Zurich
Switzerland

Eloísa Martínez Viviente
Laboratory of Inorganic Chemistry
ETHZ HCI Hönggerberg
8093 Zurich
Switzerland

1
NMR Spectroscopy and Homogeneous Catalysis

Eloísa Martínez Viviente, Paul S. Pregosin, and Daniele Schott

1.1
Introduction

NMR spectroscopy continues to develop and refine new techniques and, consequently, has become an indispensable tool in connection with solution studies in the area of homogeneous catalysis. Since the soluble catalyst precursors in transition metal catalyzed reactions often contain a variety of atoms from differing parts of the Periodic Table, it is not surprising that a multinuclear NMR approach plays an important role. Although ^{1}H NMR is still prevalent, ^{13}C (for metal carbonyls, metal carbenes, metal acyls…etc.), ^{31}P (for phosphine-based catalysts), ^{19}F (for fluorous catalysts), and occasionally even the metal center itself, are all routinely measured. Admittedly, the NMR approach to obtaining these data no longer relies solely on 1-D measurements. A variety of two-dimensional methods, using either one, two or three-bond coupling constants allow the data to be accessed in a much more efficient manner. As examples, Figure 1.1 shows: (a) part of the ^{13}C,^{1}H correlation for the Ru(II) dialkyl, π-arene compound, **1** [1], showing the relatively low frequency positions of the three-coordinated biaryl CH-resonances; (b) a section of the long-range carbon-proton correlation for the zirconium polymerization catalyst precursor, **2**, using $^{3}J(^{13}C,^{1}H)$ [2]. The observed δ values suggest some π-interaction from the five-membered ring; (c) the use of $^{3}J(^{31}P,^{1}H)$ in the chiral Pd(II) Duphos complex, **3** [3]; and (d) the ^{103}Rh resonance, for the Biphemp-based hydrogenation catalyst precursor, **4**, via $^{3}J(^{103}Rh,^{1}H)$ [4].

In addition to chemical shifts, δ, and coupling constants, J, relaxation time data, e. g., T_1, and, increasingly, diffusion constants, D, are being used to help solve selected structural problems. Although line widths in connection with variable temperature studies are still used to calculate rate constants for processes involving catalysts or intermediates which are dynamic on the NMR time scale, magnetization transfer and, especially, phase sensitive nuclear Overhauser effect (NOE) methods are often the method(s) of choice. These NMR techniques are somewhat more demanding; nevertheless, they are finding increasing acceptance. Further, additional

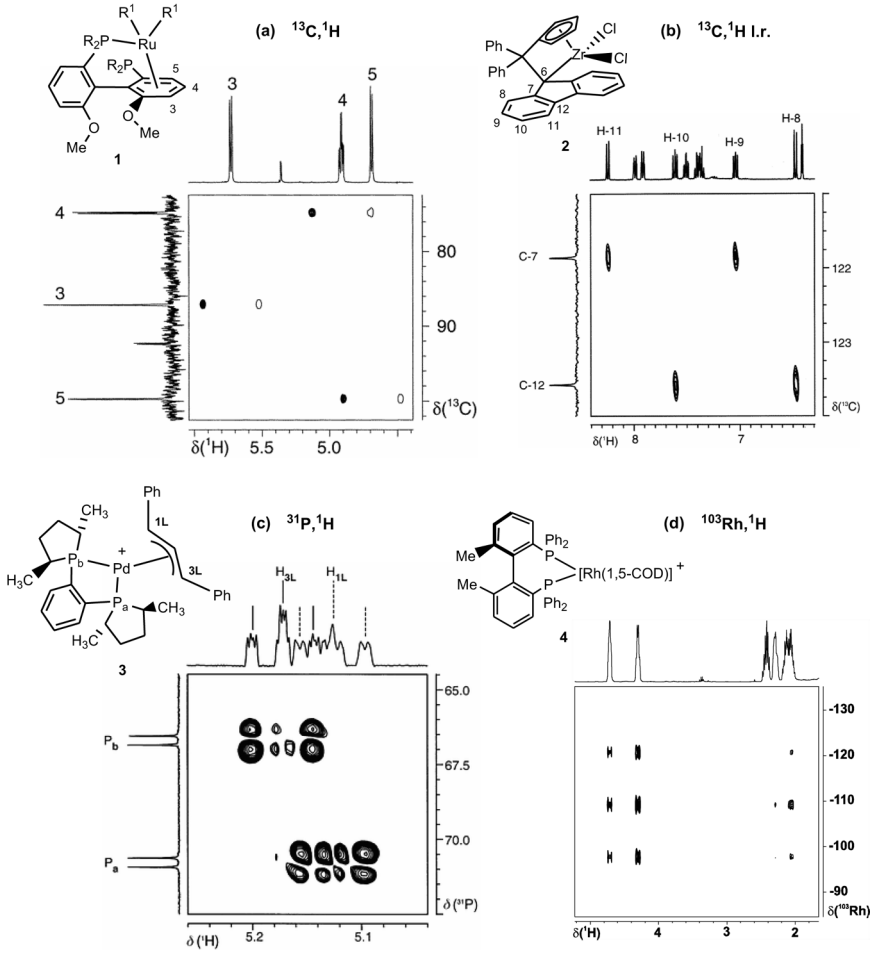

Figure 1.1 (a) Section of the phase-sensitive $^{13}C,^{1}H$ correlation for **1**, $R^1 = CH_3$, R = 3,5-di-*tert*-butylphenyl, showing the relatively low frequency positions of the three coordinated biaryl CH-resonances. The open and closed cross-peaks reflect the phases. (b) Section of the $^{13}C,^{1}H$ long-range correlation for Zr ansa-fluorenyl-complex, **2**, showing the assignment of the fluorenyl carbons, C-7 and C-12. Each of these carbons shows two correlations stemming from the values $^{3}J(^{13}C,^{1}H)$. (c) $^{31}P,^{1}H$ correlation showing the cross-peaks which help to identify the two terminal allyl protons of [Pd(η^3-PhCHCHCHPh)(Me-Duphos)](OTf), **3**. These terminal allyl protons, which correlate to their respective pseudo-trans P-atoms, appear as triplets (similar $^{3}J(^{31}P,^{1}H)$ and $^{3}J(^{1}H,^{1}H)$ values) further split by long-range proton–proton and proton–phosphorus interactions. (d) The $^{103}Rh,^{1}H$ correlation for **4**, showing selective contacts to the two olefinic protons at δ 4.31, and δ 4.72 (one stronger than the other) and an aliphatic proton of the 1,5-COD (there is also a very weak aliphatic second contact). The multiplicity in the rhodium dimension arises due to the two equivalent ^{31}P atoms coordinated to the rhodium.

tools such as: (a) parahydrogen-induced polarisation (PHIP), which may allow one to detect species present in solution at relatively low concentration, (b) high pressure measurements, which simulate catalytic conditions, and (c) NOESY measurements, which allow the determination of 3-D solution structures, are all slowly moving from the hands of the NMR specialist to the practising catalyst chemist. In the following pages we will try to illustrate and summarise some of the more relevant applications of all of these methods.

1.2 Reaction Mechanisms via Reaction Monitoring

Following the course of a reaction by NMR remains one of the most popular applications of this technique in homogeneous catalysis. The resulting kinetic information and/or the detection and identification of intermediates are important sources of mechanistic information. Often, isotopic labeling with ^{2}H [5–12] or ^{13}C [13–15] facilitates the acquisition and interpretation of the resulting NMR spectra.

1.2.1 Detecting Intermediates

A number of compounds can be recognized in the hydrogenation of ^{13}C labeled MAC (methyl-(*Z*)-α-acetamidocinnamate, 50 % ^{13}C in the α-olefin carbon) using the model Rh catalyst, $[Rh(diphos)(MeOH)_2]^+$, **5** [16, 17]. Figure 1.2 shows the proposed catalytic cycle and the most relevant sections of the various NMR spectra of **6** and **7**. The ^{31}P spectrum of **6** was measured at 233 K and shows the ^{13}C satellites for P_A (the larger ^{31}P–^{13}C coupling is associated with the trans-geometry). The ^{13}C NMR spectrum of the α-carbon of **7** (intercepted at –78 °C) clearly reveals that H transfer during the migratory insertion step occurs at the β-carbon atom of the C=C bond, leaving the α-carbon atom bonded to the Rh ($^{1}J(^{103}Rh,^{13}C(\alpha))$ = 21 Hz). The increased ^{13}C S/N and additional spin–spin interactions provided by the ^{13}C labeling are important for the assignment. Monitoring studies on the last step of the cycle via ^{31}P and ^{1}H NMR allowed the determination of a first-order rate law and the activation parameters.

In a related study using the chelating phosphine chiraphos, several species, **8**–**10**, were recognized by ^{31}P NMR (see Figure 1.3) [18]. Only a single diastereomer, **10**, forms, indicating that the binding is stereospecific.

The catalytic cycle for the Rh-catalyzed 1,4-addition of phenylboronic acid to an α,β-unsaturated ketone could be nicely described by in situ ^{31}P NMR (see Figure 1.4) [19]. The three {*S*}-Binap species $RhPh(PPh_3)$(Binap), **11**, Rh(oxaallyl)(Binap), **12** and $[Rh(OH)(Binap)]_2$, **13**, have all been detected. Complex **11** affords a modestly complicated spectrum (see spectrum A), due to the ABMX spin system. The oxa-allyl complex, **12**, in spectrum B exists in two diastereomeric forms (with overlapping signals between 48 and 49 ppm). The resonances for the bridging hydro-

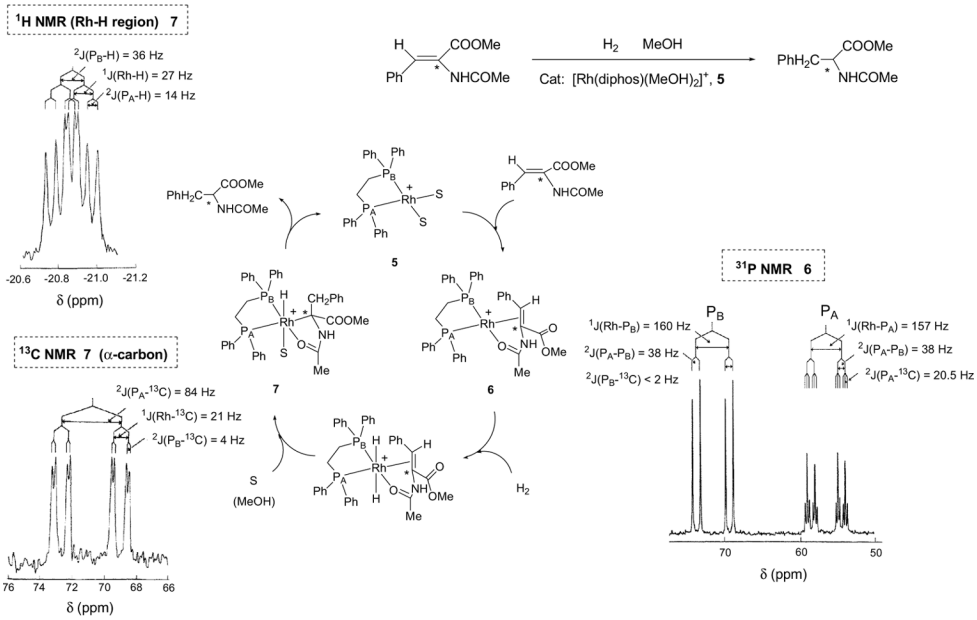

Figure 1.2 Catalytic cycle for the Rh-catalyzed hydrogenation of methyl-(*Z*)-α-acetamidocinnamate, (50 % ^{13}C in the α-C, denoted by *) in MeOH.

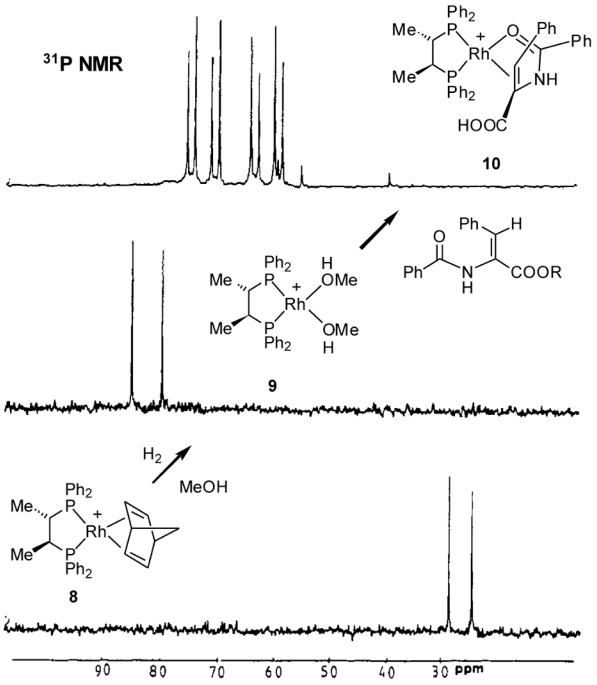

Figure 1.3 Stable intermediates in the enamide hydrogenation by (*S*,*S*)-*trans*-bis(2,3-diphenylphosphinobutane)rhodium, detected by ^{31}P NMR. The various multiplicities arise from $^{1}J(^{103}\mathrm{Rh},^{31}\mathrm{P})$ and $^{3}J(^{31}\mathrm{P},^{31}\mathrm{P})$.

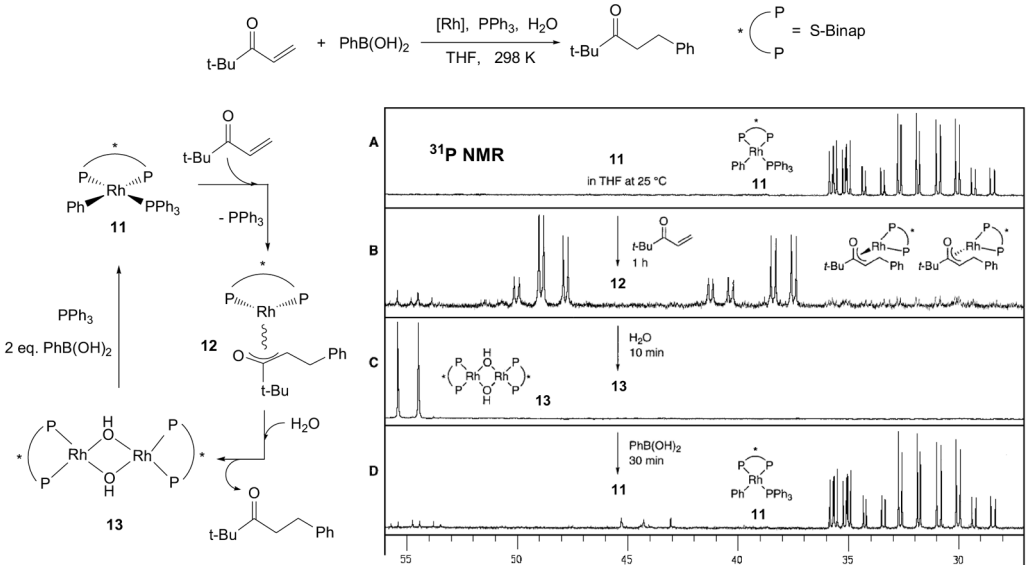

Figure 1.4 Mechanistic aspects of the Rh-catalysed 1,4-addition of phenylboronic acid to an α,β-unsaturated ketone, monitored by ^{31}P NMR.

xide **13**, with equivalent P-atoms, are observed, in spectrum C, at ca. 55 ppm. The starting PPh_3 complex, **11**, is regenerated in spectrum **D**.

In the zirconocene-catalyzed polymerization of alkenes, Landis and coworkers [20] have reported in situ observation of a Zr-polymeryl species, **15**, at 233 K (Figure 1.5). Complex **15** is formed by partial reaction of **14** with excess 1-hexene. Derivatives **16** and **17** are generated quantitatively from **15** by addition of ca. 10 equiv. of propene and ethene, respectively. No other intermediates, such as alkene complexes, secondary alkyls, diasteromers of **15** or **16**, or termination products, accumulate to detectable levels. These NMR studies permit direct monitoring of the initiation, propagation and termination processes, and provide a definitive distinction between intermittent and continuous propagation behavior.

Espinet and coworkers [21] have captured an NMR "snapshot" of a catalytic cycle for the Stille reaction, involving compounds **18–22** (see Figure 1.6). The vinylic region of the ^{1}H and $^{1}H\{^{31}P\}$ NMR spectra of **19–22** is shown. Both Pd(II) Pd(vinyl)R(PP), **20** and Pd(0) Pd($RCH{=}CH_2$)(PP), **21** species were identified.

Brown and coworkers [22] have studied the Pd-catalyzed Heck arylation of methyl acrylate via ^{31}P and ^{13}C NMR (see Figure 1.7). Reaction of the aryl iodide complex **23** with AgOTf (THF, 195 K) gives the THF and aquo-complexes **24** and **25**, respectively, which were detected via ^{31}P NMR below 203 K. Addition of H_2O to the sample shifts the equilibrium towards **25**, pointing to an existing fast exchange between solvates **24** and **25**. Reaction of **24**/**25** with 3-$\{^{13}C\}$ labeled methyl acrylate (20-fold excess, 213 K) affords the insertion product **26**. Warming to 233 K leads to the formation of **27**, which is in turn converted into **29**, stable to

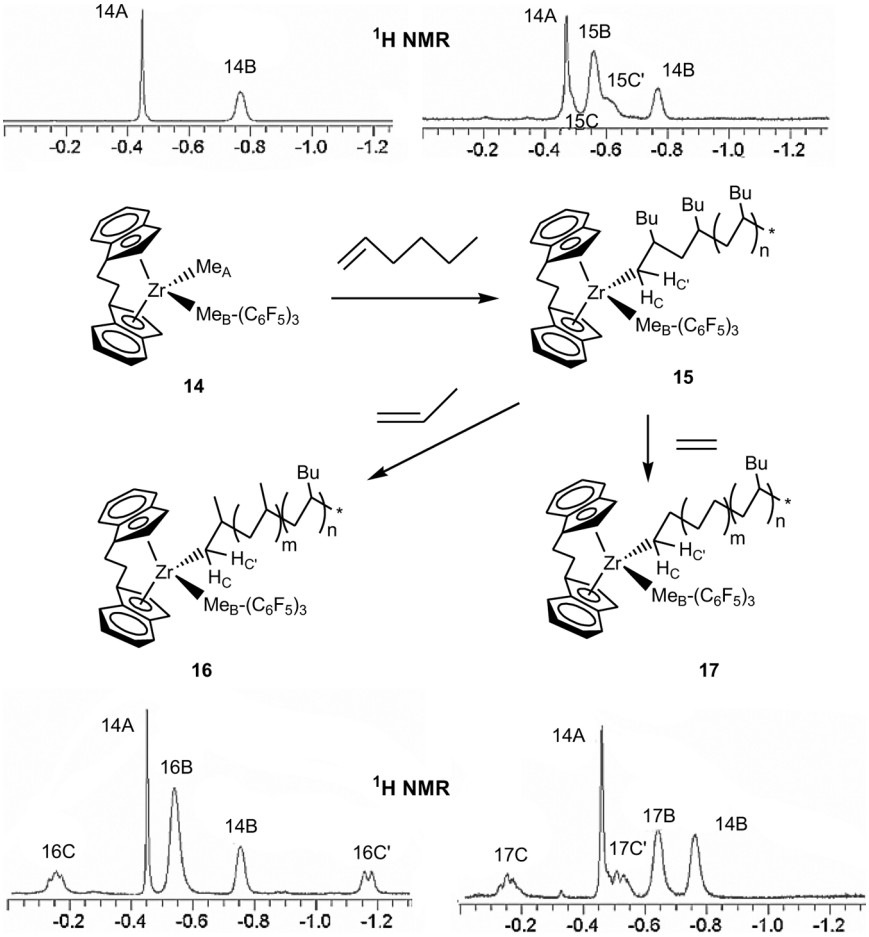

Figure 1.5 *In situ* Detection of Zr-polymeryl species by ^{1}H NMR (233 K, d^8-toluene). Only the region between 0 and -1.3 ppm is shown, in which resolved resonances for the diastereotopic Zr–CH_2–POL protons and the Zr–Me–B groups are detected.

273 K. The rearrangement from **27** to the more stable, primary alkyl regioisomer **29** was shown to be intermolecular. This is thought to occur via the unobserved hydride **28**, since addition of unlabeled methyl acrylate leads to the equilibrium distribution of ^{13}C label in **29** (**28** exchanges acrylate ligands with the acrylate pool).

Using ^{31}P NMR the same authors have identified several intermediates in the asymmetric Heck arylation of dihydrofuran [23, 24]. Reaction of the Binap salt, **30**, with 2,3-dihydrofuran below 233 K gave salt **31** as the single species (see Figure 1.8). A parallel reaction between **30** and [2-^{2}H] 2,3-dihydrofuran confirmed the structure. At 243 K, **31** slowly decomposed to form **32** and **32'** with concomitant release of the coupling product **33** (91 % ee).

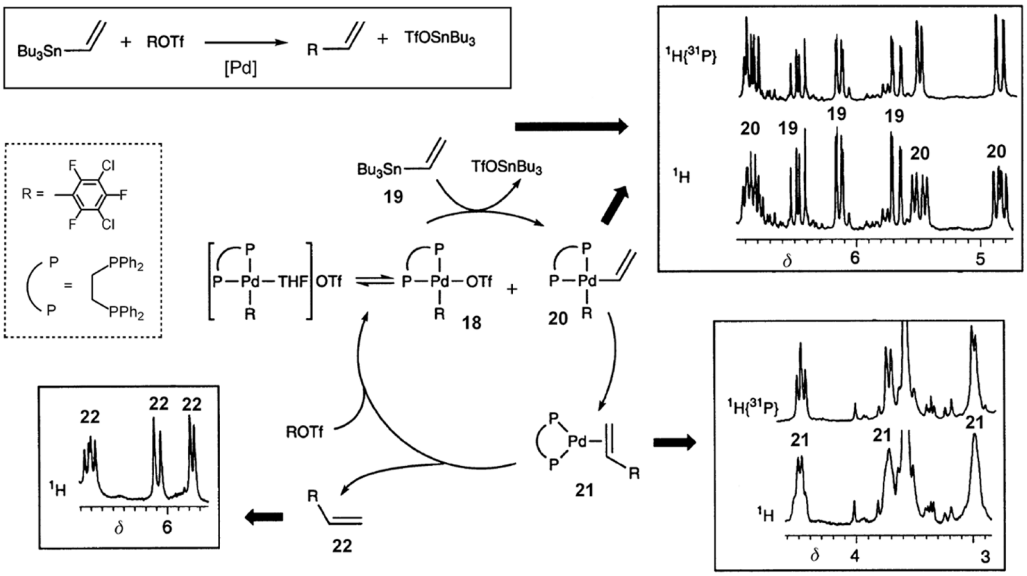

Figure 1.6 Catalytic cycle for a Stille reaction showing the vinylic regions of the ^{1}H and $^{1}H\{^{31}P\}$ NMR spectra of the products detected in situ (in d^{8}-THF).

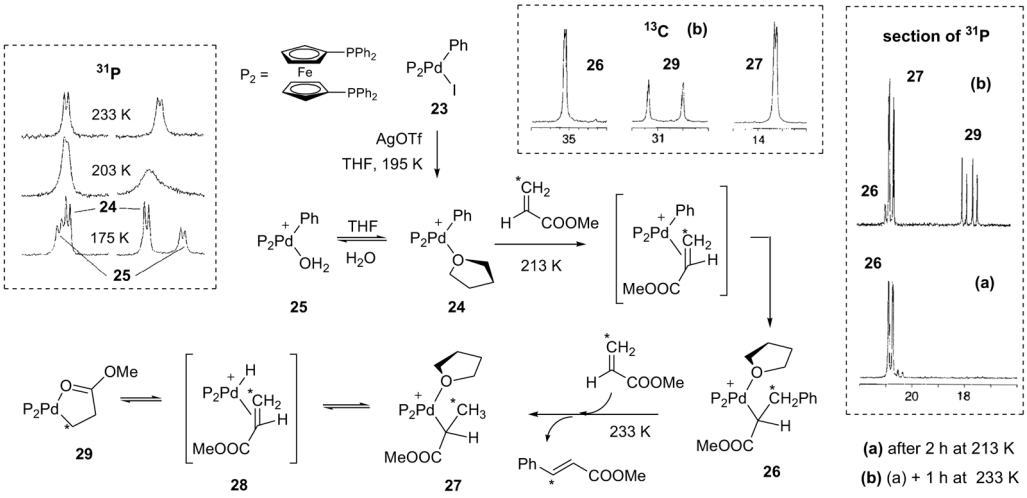

Figure 1.7 NMR investigation on the Heck reaction. The ^{31}P NMR spectra on the right show the low-frequency region.

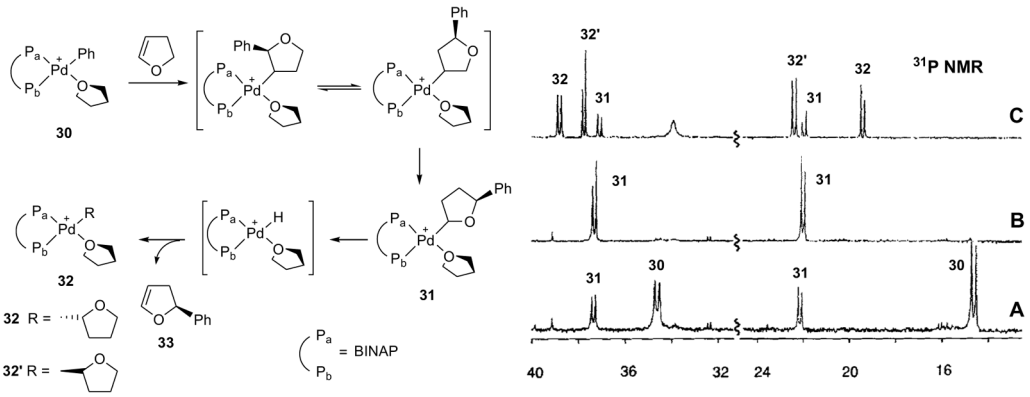

Figure 1.8 ^{31}P NMR spectra of the reaction sequence between **30** and 2,3-dihydrofurane. Spectrum A: partial conversion of **30** to **31** at 223 K. Spectrum B: After complete formation of **31** at 233 K. Spectrum C: nearly complete decomposition of **31** at 243 K to form **32** and **32'**. The signals at higher frequency correspond to P_a.

For the industrially important Pd-catalyzed methoxycarbonylation of ethene to methyl propanoate, all the intermediates of the cycle have been identified. Starting from **34**, $^{13}CH_2{=}CH_2$ and ^{13}CO, the process has been shown to proceed via a hydride rather than a methoxycarbonyl cycle (Scheme 1.1) [25][26]. Figure 1.9 shows the ^{31}P NMR spectrum at 193 K of a 1:1 mixture of the two isotopomers **35a** and **35b**, formed in the reaction of **34** with $^{13}CH_2{=}^{12}CH_2$. The presence of an agostic interaction is supported by the ^{13}C chemical shifts ($\delta(CH_2)$ 31, and $\delta(CH_3)$ 8), which are reversed with respect to classical Pd-ethyl complexes.

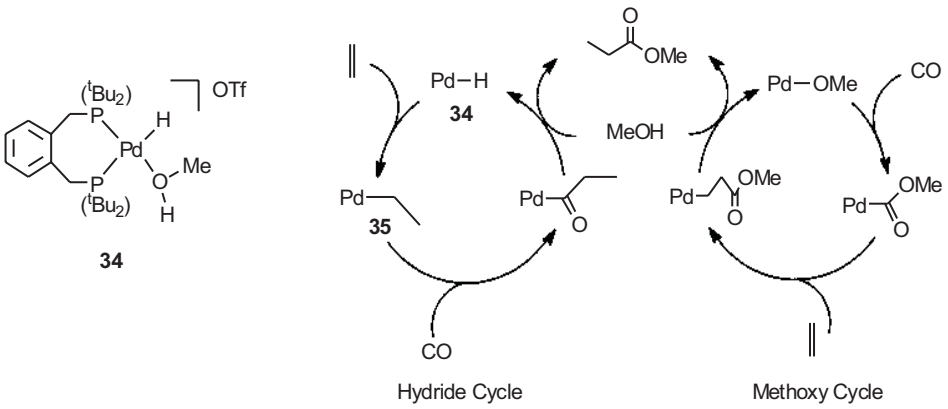

Scheme 1.1 The two possible mechanisms for the Pd-catalysed methoxycarbonylation of ethene.

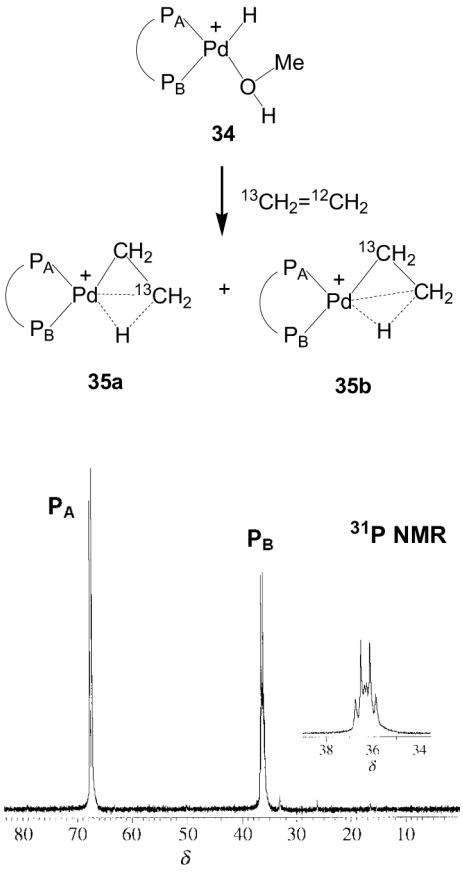

Figure 1.9 ^{31}P NMR spectrum at 193 K of a 1:1 mixture of the two isotopomers $[Pd(L–L)(CH_2{}^{13}CH_3)]^+$, **35a**, and $[Pd(L–L)(^{13}CH_2CH_3)]^+$, **35b**, formed in the reaction of **34** with $^{13}CH_2{=}^{12}CH_2$. For **35a**, the phosphorus trans to the ethyl group (P_B δ 36.1) couples with the cis-phosphorus P_A [δ 68, $^2J(^{31}P_A,^{31}P_B)$ 31 Hz], while the $^2J(^{31}P_B,^{13}C)$ is not observed due to the low natural abundance of ^{13}C. In **35b**, however, the coupling of P_B with both P_A and the labelled trans carbon atom [$^2J(^{31}P_B,^{13}C)$ 38 Hz] can be observed, resulting in a doublet of doublets, which is superimposed with the doublet originating from **35a**.

In situ NMR studies on analogous Pt catalysts for the methoxycarbonylation reaction reveal CO trapping at *every* step in the catalytic cycle of the active intermediates (Figure 1.10) [27]. This explains the observed slow kinetics. Thus, **36** reacts with ^{13}CO in CH_2Cl_2 at 193 K to form only $[Pt(L–L)(C_2H_5)(^{13}CO)]^+$, **37**, which upon warming to ambient temperature in the presence of excess CO affords $[Pt(L–L)(^{13}C(O)Et)(^{13}CO)]^+$, **38**. This transformation is *reversible*, and both compounds have been detected by in situ $^{13}C\{^1H\}$ NMR spectroscopy.

1.2.2
Reaction Kinetics via NMR

The previous section focused on the detection of intermediates in a catalytic reaction, thereby affording an "NMR picture" of the several steps involved in the mechanism. Occasionally, NMR can be a convenient tool for monitoring reaction rates provided that the reaction is slow enough for a series of 1D spectra to be acquired during its course.

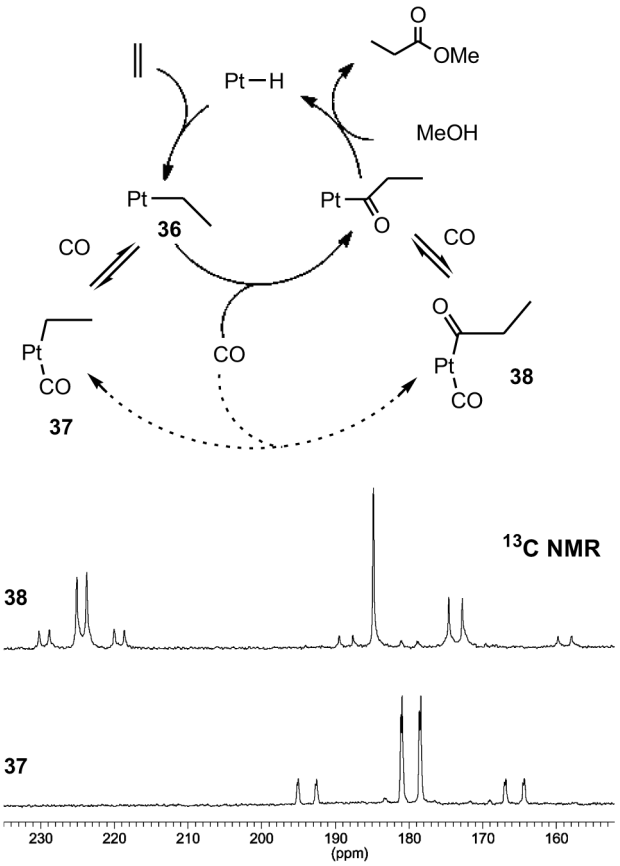

Figure 1.10 Pt-catalysed methoxycarbonylation of ethene, studied by ^{13}C NMR.

Figure 1.11 provides an example of ^{1}H NMR monitoring in the Pd-catalyzed cycloisomerization of dimethyl diallyl malonate, **39** [28]. The kinetic profile reveals a pronounced induction period after which the exocyclic alkene **40a** is formed predominantly as the kinetic product. A hydropalladation mechanism was proposed on the basis of NMR experiments, and the transient species **41**, formed by allylpalladation of the coordinated diene, could be detected and identified with the help of ^{2}H and ^{13}C labeling. The hydride Pd catalyst, **42**, would be generated from **41** by water-promoted β-hydride elimination. The observed induction period is associated with the formation of the Pd-hydride **42**.

In the oxidative addition of a fluorinated aryl iodide, **43**, to "$Pd(PPh_3)_2$" (Figure 1.12) [29], ^{19}F NMR has been used to follow the cis-to-trans isomerization of the cis-bis-phosphine product, **44**, to the trans-isomer, **45**. The ^{19}F NMR kinetic study reveals a first order dependence for the rate of isomerization on the concentration of **44**. An application of a ^{19}F NMR kinetic study to the evaluation of the

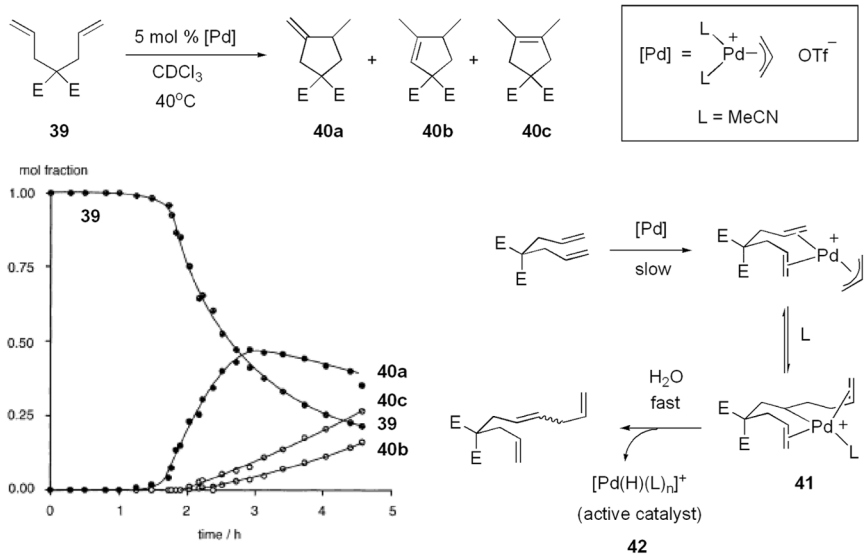

Figure 1.11 Pd-catalysed cycloisomerisation of dimethyl diallyl malonate. Kinetic profile based on ^{1}H NMR, and proposed reaction mechanism.

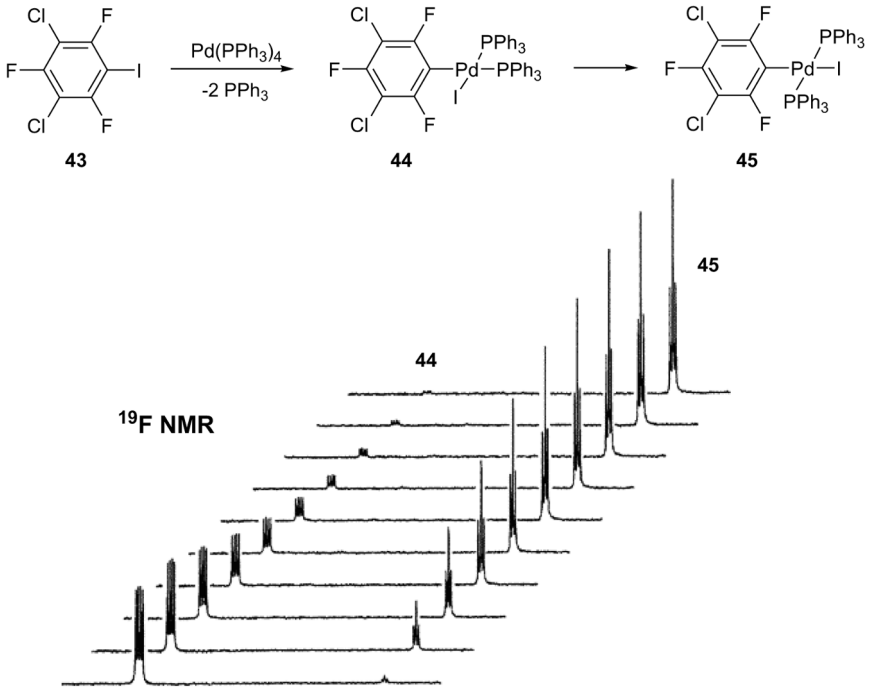

Figure 1.12 ^{19}F NMR study of the cis-to-trans isomerization of **44** to **45**. Only the ortho ^{19}F resonances are shown. In **44**, the coupling with two inequivalent ^{31}P atoms affords a doublet of doublets. For **45**, the spectrum consists of a triplet.

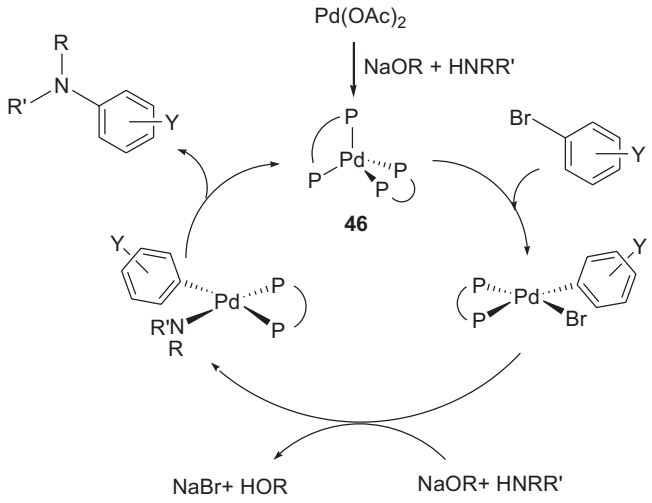

Scheme 1.2 Pd-catalysed amination of aryl halides using the chiral ligand Binap.

factors contributing to the "copper effect" in the Stille reaction has also been reported [30].

In the Pd-catalyzed amination of aryl halides using Binap, the Pd(0) complex $Pd(Binap)_2$, **46**, has been identified by ^{31}P NMR as the resting state in the catalytic cycle (Scheme 1.2) [31]. The zero-order dependence of the reaction rate on the amine concentration has been confirmed via a ^{1}H NMR study with primary amines (Figure 1.13, left). For secondary amines, however, a first-order dependence on amine was apparent (Figure 1.13, right), suggesting a change in the resting state of the catalyst to one that would react with the amine. ^{31}P monitoring of the catalyst concentration (Figure 1.13, center) showed a gradual consumption of **46** in the reaction with the secondary amine, but not with the primary, explaining the different kinetic behavior.

We note that there are NMR-based kinetic studies on zirconocene-catalyzed propene polymerization [32], Rh-catalyzed asymmetric hydrogenation of olefins [33], titanocene-catalyzed hydroboration of alkenes and alkynes [34], Pd-catalyzed olefin polymerizations [35], ethylene and CO copolymerization [36] and phosphine dissociation from a Ru-carbene metathesis catalyst [37], just to mention a few.

Finally, an example of reaction monitoring with a "rare" nucleus: Figure 1.14 reproduces three sequences of ^{11}B NMR spectra of the Zr-catalysts **47**-**49**/MAO (MAO = methylaluminoxane) during the polymerization of ethylene [38]. No changes are detected in the systems **47**/MAO (a) and **49**/MAO (c) during the course of reaction; however, for **48**/MAO in (b), a new ^{11}B signal appears. This is attributed to an exchange of the boron benzyloxy substituent of **48** with the methyl from the MAO, effectively transforming **48** into **49**. This transformation of the catalyst is thought to explain why the selectivity of the **48**/MAO system